Published in final edited form as:
AJR Am J Roentgenol. 2013 November ; 201(5): W698–W706. doi:10.2214/AJR.12.9698.

PET With ^{62}Cu-ATSM and ^{62}Cu-PTSM Is a Useful Imaging Tool for Hypoxia and Perfusion in Pulmonary Lesions

Tian Zhang[1], **Shiva K. Das**[2], **Diane R. Fels**[3], **Katherine S. Hansen**[4], **Terence Z. Wong**[5], **Mark W. Dewhirst**[2], and **Gordana Vlahovic**[1]

[1]Division of Medical Oncology, Department of Medicine, Duke University Hospital, Rm 047 Baker House, Trent Dr, DUMC 3624, Durham, NC 27710

[2]Department of Radiation Oncology, Duke University Medical Center, Durham, NC

[3]Medpace, Cincinnati, OH

[4]Department of Surgical and Radiological Science, Veterinary Medical Teaching Hospital, UC Davis School of Veterinary Medicine, Davis, CA

[5]Department of Radiology, Duke University Hospital, Durham, NC

Abstract

OBJECTIVE—Hypoxia is a characteristic of many tumors and portends a worse prognosis in lung, cervical, prostate, and rectal cancers. Unlike the others, lung cancers present a unique challenge in measuring hypoxia, with invasive biopsies and higher rates of complications. Noninvasive imaging studies detecting hypoxia using isotopes of copper-diacetyl-bis(N4-methylthiosemicarbazone) (^{62}Cu-ATSM) have predicted prognosis and treatment outcomes in some small feasibility trials. These images, however, may not identify all areas of hypoxia. Hence, we hypothesize that the addition of another PET imaging agent, copper-pyruvaldehyde-bis(N4-methylthiosemicarbazone) (^{62}Cu-PTSM), which can detect areas of perfusion, can augment the information obtained in ^{62}Cu-ATSM PET scans.

SUBJECTS AND METHODS—To characterize tumors on the basis of both perfusion and hypoxia, 10 patients were studied using both ^{62}Cu-ATSM and ^{62}Cu-PTSM PET scans. In addition, proteomic arrays looking at specific proangiogenic, survival, and proinflammatory targets were assessed.

RESULTS—Six of 10 patients had evaluable PET scans. Our initial experience of characterizing lung tumor hypoxia using ^{62}Cu-ATSM and ^{62}Cu-PTSM PET scans showed that visualization of areas with hypoxia normalized for perfusion is feasible. All studied tumors exhibited some hypoxia. Despite the small sample size, a positive relationship was noted between epidermal growth factor levels and ^{62}Cu-ATSM-detected hypoxia.

CONCLUSION—This initial series of ^{62}Cu-ATSM and ^{62}Cu-PTSM PET scans shows that evaluating lung masses by visualizing hypoxia and perfusion is a feasible and novel technique to provide more information. Further investigation is warranted to assess the potential role of ^{62}Cu-

Address correspondence to G. Vlahovic (gordana.vlahovic@dm.duke.edu).

ATSM and ^{62}Cu-PTSM PET techniques combined with proteomics as alternatives to invasive biopsy techniques in clinical care.

Keywords

hypoxia; lung tumor; perfusion; PET

Lung cancer has the highest cancer-related mortality and is the second most common malignancy in both men and women in the United States, with more than 160,000 deaths and 226,000 new cases in 2012 [1]. Mortality from lung cancer is high; even patients diagnosed with stage I non–small cell lung cancer have a 5-year survival rate of less than 70%.

Hypoxia is a common characteristic of most solid tumors, including lung, head and neck, cervical, and breast cancers [2]. The tumor microenvironment has areas of both chronic hypoxia (low perfusion and oxygen permeation at all times) and cycling hypoxia (intermittent low oxygen transport) [3]. Both types of hypoxia are known to induce resistance to treatment, enhance tumor progression, and ultimately reduce patient survival [2]. Importantly, hypoxia upregulates hypoxia-inducible factor 1 (HIF-1)–dependent pathways that promote adaptation to low oxygen availability. HIF-1 activates more than 70 genes involved in anaerobic glycolysis, oxidative stress response, angiogenesis, and tumor progression [4]. Recently, levels of carbonic anhydrase isoform IX, an HIF-1–dependent cell transporter protein involved in pH regulation, have been associated with a worse prognosis in patients with early-stage non–small cell lung cancer [5]. Many proteins, such as plasminogen activator inhibitor–1 and vascular endothelial growth factor (VEGF), are upregulated with HIF-1 induction in tumor hypoxia; these proteins may be useful as serum biomarkers for detecting treatment responses as well as disease progression [4].

Fluorine-18-FDG PET scan is currently the most efficacious way to detect and monitor malignancies, including lung tumors, during therapy. However, both malignant tumors and benign conditions, such as granulomatous disease and infectious disorders, can show avidity on FDG PET, so it is often difficult to distinguish malignancies from false-positive conditions. To improve radiographic specificity for malignant tumors, hypoxia, one of the hallmarks of malignancy, has been recognized as a potential imaging target.

Recently, novel molecular imaging techniques using copper-diacetyl-bis(N4-methylthiosemicarbazone) (^{62}Cu-ATSM) have been used to image tissue hypoxia [6]. These techniques take advantage of several positron-emitting copper isotopes, including ^{60}Cu, ^{61}Cu, ^{62}Cu, and ^{64}Cu [7–9], which vary in positron energy and half-life. The shorter lived isotopes, ^{60}Cu and ^{62}Cu, with half-life periods of 23.4 and 9.7 minutes, respectively, are typically used clinically. Copper-64 has a 12.3-hour half-life, making it more suitable for preclinical studies [10].

Copper-pyruvaldehyde-bis(N4-methylthiosemicarbazone) (^{62}Cu-PTSM) is reduced readily by the mitochondria, is retained in most tissues, and, thus, can be used as a marker of tissue perfusion [9]. ^{62}Cu-ATSM is an analog of ^{62}Cu-PTSM but has a lower redox potential,

allowing ^{62}Cu-ATSM to be selectively reduced in hypoxic cells, where it is trapped and used in cellular macromolecules [11].

PET with these radioisotopes has been studied in a variety of clinical trials. Although many of these trials examine tumor hypoxia by using ^{62}Cu-ATSM, they do not concurrently image tumor perfusion. The uptake of ^{62}Cu-ATSM has been evaluated as an imaging marker of hypoxia and is associated with different treatment outcomes in lung and cervical cancer. In one study, ^{62}Cu-ATSM uptake was strong in six patients with lung cancer, compared with very minimal lung uptake in four healthy control subjects. In addition, ^{62}Cu-ATSM did not have the same distribution of uptake as FDG, confirming that areas of tumor hypoxia and low blood flow do not have high levels of metabolic activity [12]. Furthermore, an inverse relationship has been observed between ^{60}Cu-ATSM uptake and progression-free survival in 38 patients with locally advanced cervical cancer [13]. Indeed, in 19 other patients with lung cancer, treatment responses were more likely to occur in patients whose tumors exhibited less hypoxia with lower ^{60}Cu-ATSM uptake [14]. These studies have shown the feasibility of using ^{60}Cu-ATSM PET scans in following up treatment responses; however, they have not explored the dependence that this marker of hypoxia has on tumor perfusion.

To exploit the clinical potential of hypoxia as a prognostic biomarker or therapeutic target, our group previously reported a proof-of-concept study showing the difference in ^{62}Cu-PTSM and ^{62}Cu-ATSM accumulation between two patients with solitary lung nodules, one with malignant adenocarcinoma and another with a benign granuloma [15]. We then hypothesized that these imaging studies would be feasible for characterization of locally advanced lung cancer according to tissue hypoxia and perfusion. The current study investigates the feasibility and utility of the novel imaging techniques of both ^{62}Cu-ATSM and ^{62}Cu-PTSM PET to characterize both tissue hypoxia and perfusion. In addition, plasma samples were collected from patients for proteomic analysis; these proteomics results were correlated with those obtained from hypoxia imaging studies.

Subjects and Methods

^{62}Cu-PTSM and ^{62}Cu-ATSM Synthesis

On the day of each scan, ^{62}Cu isotope was obtained from a ^{62}Zn/^{62}Cu minigenerator (PDI, Proportional Technologies). Then, radiolabeled ^{62}Cu-ATSM and ^{62}Cu-PTSM compounds were produced using a rapid synthesis kit (^{62}Cu-BTS kit, Proportional Technologies). The Duke Medical Center Radioactive Drug Research Committee approved the use of ^{62}Cu-ATSM and ^{62}Cu-PTSM for human research.

Patients

Patients were recruited at Duke University Medical Center after referral to the study by their surgeon or medical oncologist. Patients who enrolled in this study had either histologically confirmed malignancy or a greater than 75% likelihood of malignancy by expert agreement from a multidisciplinary team of thoracic surgeons and thoracic medical oncologists (the principal investigator). Inclusion criteria included age greater than or equal to 18 years, Eastern Cooperative Oncology Group performance status 0–2 (Karnofsky score, > 60%),

normal renal (estimated glomerular filtration rate > 60 mL/min) and bone marrow (absolute neutrophil count > 1500 cells and platelet count > 100,000) function, eligibility for surgical resection (limited disease on imaging studies and negative mediastinoscopy), and ability to understand the informed consent. Exclusion criteria included chemoradiotherapy within the past year, uncontrolled diabetes mellitus, and pregnancy. The Duke University Medical Center institutional review board approved the clinical protocol, and patients signed the written informed consent before participating in this imaging study.

PET

Patients initially underwent unenhanced CT of the chest with the patient in quiet end-expiration. CT scans with parameters of 3.75-mm slice thickness, pitch of 1.375:1, table speed of 27.5 mm per rotation, and rotation time of 0.5 second were obtained with acquisition times of less than 10 seconds.

A PET/CT scanner with a 16-MDCT unit (Discovery ST, GE Healthcare) was used for PET. All PET examinations were corrected on the basis of CT attenuation. PET images were acquired in the 2D mode and were reconstructed using ordered subset expectation maximization (30 subsets and two iterations) with a 50-cm diameter FOV and 128 × 128 matrix.

Patients underwent PET with FDG using a routine clinical protocol after a 4-hour fast. Patients were injected with FDG (mean dose, 12.8 ± 2.4 mCi [473.6 ± 88.8 MBq]). FDG PET was performed 1 hour after FDG injection. Patients who had already undergone PET were not required to undergo another FDG scan.

Patients were injected first with the radioactive tracers ^{62}Cu-PTSM (mean dose, 10.9 ± 4.4 mCi [403.3 ± 162.8 MBq]) followed by ^{62}Cu-ATSM (mean dose, 11.5 ± 3.4 mCi [425.5 ± 125.8 MBq]) with a minimum separation time of 50 minutes to allow radioactive decay of the previous tracer, which was consistent with protocol algorithm. Serial PET was then performed over a single bed position to include the pulmonary nodule. Dynamic PET images were acquired immediately after IV injection of each radiotracer, with frames multiplied by frame time of 12 × 10, 4 × 30, 3 × 120, and 2 × 300 seconds. Total acquisition times were 20 minutes after each injection. The ^{62}Cu-ATSM and ^{62}Cu-PTSM standardized uptake values (SUVs), obtained from the last time point when steady state values were established, were tabulated. Because there are several kinetic analysis models in the literature with varying mechanisms, with lack of validation of any of these models, we chose not to use kinetic analysis.

Normalization of ^{62}Cu-ATSM by ^{62}Cu-PTSM

Mechanistically, ^{62}Cu-PTSM leaks out of the vasculature into the extravascular space and then diffuses freely into cells, where it is irreversibly trapped by reduction and disassociation. Copper-62-ATSM behaves in much the same way, except that reduced ^{62}Cu-ATSM in the cells is reoxidized in the presence of oxygen, allowing it to diffuse out of cells. Thus, the amount of ^{62}Cu-ATSM trapped in cells by reduction and disassociation is a measure of the lack of oxygen. Assuming that the dynamics of ^{62}Cu-ATSM and ^{62}Cu-PTSM leakage from the vasculature are similar, the amount of ^{62}Cu-PTSM trapped in cells

is an indirect measure of the approximate amount of ^{62}Cu-ATSM that diffused into the cells before being either irreversibly trapped or escaping from the cell after reoxidation. It follows that the ratio of ^{62}Cu-ATSM SUV to ^{62}Cu-PTSM SUV ("normalized ^{62}Cu-ATSM") in a tumor voxel is a measure of hypoxia because it reflects the fraction of ^{62}Cu-ATSM entering the voxel that is eventually trapped. A larger ratio implies greater hypoxia. SUV is used in the normalization to scale activity by the total injected activity, which differs between ^{62}Cu-ATSM and ^{62}Cu-PTSM. Overall tumor hypoxia is defined here as the mean over all tumor voxels of the normalized ^{62}Cu-ATSM SUV (similar to mean FDG SUV being used to describe tumor glycolysis).

Surgical Resection

Patients underwent wedge resection or lobectomy at the discretion of their surgeon. All samples were sent for routine surgical pathologic analysis, and histopathologic data were obtained.

Serum Cytokine Arrays

Serum from patient blood samples obtained at the time of FDG PET scans was used to assess levels of specific protein markers. Proteomic arrays using kits from Meso Scale Discovery were performed according to the manufacturer's protocol. Kits used were the MULTI SPOT 96 4-Spot Human Hypoxia Triplex (erythropoietin, VEGF, and insulin growth factor binding protein–1), the MULTI SPOT 96 4-Spot Prototype Human Single-Plex epidermal growth factor kit, the MULTI SPOT 96 4-Spot Human ProInflammatory-4 II kit (interleukin [IL]–1β, IL-6, IL-8, and tissue necrosis factor–α), and the MULTI SPOT 96 4-Spot Human Growth Factor I kit (basic fibroblast growth factor, soluble FMS-like tyrosine kinase 1, placental growth factor, and VEGF). All 96-well plates were read using the SECTOR Imager in the Duke Proteomics Core Facility.

Statistical Analysis

The ratio of ^{62}Cu-ATSM to ^{62}Cu-PTSM was calculated as the mean of ^{62}Cu-ATSM to ^{62}Cu-PTSM ratios over all tumor voxels. For the imaging portion of this study, descriptive statistics were used to report calculated SUVs and ratios in relation to the size and pathologic profile of each patient's pulmonary lesion. Basic statistics were performed for calculation of the reported correlation values in the cytokine array data.

Results

Patient Characteristics

From April 2, 2008, until September 8, 2008, a total of 10 patients were enrolled in this study. Results from the first two patients were reported previously [15]. Of the other eight patients, one patient did not tolerate the procedure because of claustrophobia and therefore did not undergo all sequences of PET. Longer acquisition sequences than initially projected were used in analysis, and, thus, scans from only six patients were available for comprehensive analysis. Patient characteristics (including those reported previously) are presented in Table 1.

Patients were all in the sixth to eighth decades of life. Eight of 10 patients were men, and two were women. All patients had initial studies that showed high suspicion for malignancy, with high FDG uptake on FDG PET (SUV range, 5.5–17.6), and subsequently underwent surgical resection. On pathologic analysis, eight patients had malignancies: six patients had adenocarcinoma of the lung, one had sarcomatoid carcinoma of the lung, and another had metastatic head and neck squamous cell carcinoma. One patient had a benign granuloma, as previously reported, and the final patient had pulmonary Langerhans cell histiocytosis.

^{62}Cu-ATSM and ^{62}Cu-PTSM PET Scans

For all six study patients, FDG PET and both ^{62}Cu-ATSM and ^{62}Cu-PTSM PET scans were acquired (Table 2). The ratio between ^{62}Cu-ATSM and ^{62}Cu-PTSM was computed as the sum of all the ratios for all voxels divided by the number of voxels (Table 3). Figure 1 is a representative image of patient 3, with stage IV lung adenocarcinoma and bilateral lung nodules on presentation. Patient 3 also had the second highest amount of tumor hypoxia as detected in the ratio between ^{62}Cu-ATSM and ^{62}Cu-PTSM.

Figure 2A shows representative images from patient 5, who had stage III sarcomatoid carcinoma of the lung. In this patient's scans, the highest ratio of ^{62}Cu-ATSM to ^{62}Cu-PTSM was found, indicating the highest levels of hypoxia. Patient 6 had stage III adenocarcinoma of the lung in the right lower lobe and the third highest levels of hypoxia, as depicted in Figure 3. The patient with pulmonary Langerhans cell histiocytosis had the second lowest levels of hypoxia (Fig. 4). We did not find the same difference between hypoxia detected in patients with malignancies and that detected in the patient with pulmonary Langerhans cell histiocytosis as we found between adenocarcinoma and granuloma in our initially published work.

Of the last two patients who were enrolled, both had adenocarcinoma on pathologic analysis, stage II and I, respectively, with the least tumor hypoxia on ^{62}Cu-ATSM and ^{62}Cu-PTSM PET scans on the former and the second-highest levels of tumor hypoxia on ^{62}Cu-ATSM and ^{62}Cu-PTSM PET scans in the latter (not depicted).

Figure 5A displays ^{62}Cu-ATSM and ^{62}Cu-PTSM (divided by their respective injected activities) as a function of distance from the center of the tumor, as imaged in patient 5. Both ^{62}Cu-ATSM and ^{62}Cu-PTSM levels increase as distance increases from the center of the tumor. This is as expected for ^{62}Cu-PTSM, because greater peripheral vasculature leads to greater extravascular diffusion. Contrary to expectations, ^{62}Cu-ATSM also increases toward the periphery, implying that the periphery is relatively more hypoxic than the center. Figure 5B shows ^{62}Cu-ATSM normalized to ^{62}Cu-PTSM as a function of distance. Normalized ^{62}Cu-ATSM shows an expected decreasing trend toward the periphery, because the periphery of the tumor is more perfused and therefore less hypoxic than the center. This increase in hypoxia in the periphery was only seen for patient 5, because this tumor had the largest volume of all of those scanned. The other tumors were all too small to show a trend for increased hypoxia in the tumor periphery.

Of the two patients whose PET scans were not analyzed because of technical difficulty in completing the scans, one patient had stage IV head and neck cancer, and the other patient had stage IV adenocarcinoma of the lung.

Serum Biomarkers

Candidate protein biomarkers known to be involved in tumor responses and tumor progression were studied in serum samples from all 10 patients who were initially enrolled. Figure 6 depicts the relationship of EGF plasma concentrations as a function of the ^{62}Cu-ATSM-to-^{62}Cu-PTSM ratio. As the ^{62}Cu-ATSM-to-^{62}Cu-PTSM ratio increases, as a marker of increasing hypoxia in the tumors, plasma concentrations of EGF decrease ($r = -0.87$; $R^2 = 0.76$).

Figure 7A shows VEGF and soluble FMS-like tyrosine kinase 1 concentrations for these patients; both VEGF and soluble FMS-like tyrosine kinase 1 are proteins known to be important for hypoxia adaptation. Interestingly, although higher serum levels of VEGF correlated to higher tumor hypoxia ($r = 0.22$; $R^2 = 0.05$), lower serum levels of soluble FMS-like tyrosine kinase 1 correlated to higher tumor hypoxia (Fig. 7B) ($r = -0.54$; $R^2 = 0.29$). Other potential candidate markers screened included serum proteins involved in proinflammatory stress responses, such as IL-1β, IL-6, IL-8, and tissue necrosis factor–α, as well as growth factors important for tumor survival (EGF, basic fibroblast growth factor, and placental growth factor) (not shown). No trends were found between tissue hypoxia as detected by ^{62}Cu-ATSM and ^{62}Cu-PTSM PET scans and these serum protein levels.

Patient Survival

We compiled survival data on the six patients who completed all of the PET scans (Table 3). The mean duration of follow-up was 24 months. Of the two patients with stage IV adenocarcinoma of the lung, one survived 14 months and the other survived 15 months. Another patient had stage III sarcomatoid carcinoma of the lung, the most hypoxic by ^{62}Cu-ATSM normalized to ^{62}Cu-PTSM, and also survived 5 months after diagnosis. Patient 6 had stage III adenocarcinoma, with the third highest hypoxia levels by ^{62}Cu-ATSM and ^{62}Cu-PTSM imaging, and survived only 4 months. Of the remaining three patients, patient 8 had benign pulmonary Langerhans cell histiocytosis and was alive at more than 2 years; he had the second lowest hypoxia levels by imaging. In addition, patients 9 and 10 with early-stage (stage I and II) lung adenocarcinoma were also alive at more than 2 years. The patient with stage II adenocarcinoma had the lowest hypoxia levels, and the patient with stage I adenocarcinoma had the third-lowest hypoxia levels. Taken together, it appears as though the lower hypoxia levels by ^{62}Cu-ATSM and ^{62}Cu-PTSM PET correspond to a trend toward longer survival.

Discussion

Given the difficulty and potential complications of biopsies for lung malignancies, it is important to develop noninvasive methods for stratifying patients who have cancerous lung lesions. Our results with ^{62}Cu-ATSM and ^{62}Cu-PTSM PET show the feasibility of noninvasive imaging to detect hypoxia in pulmonary lesions with short-acting radiotracers

as markers of both tissue perfusion and hypoxia. On the basis of our preliminary study of two patients, a benign granuloma was differentiated from lung adenocarcinoma with the low ^{62}Cu-ATSM uptake in the benign granuloma and high ^{62}Cu-ATSM uptake in the lung adenocarcinoma. Our current experience shows the feasibility of ^{62}Cu-ATSM and ^{62}Cu-PTSM imaging in an additional six patients with pulmonary lesions.

To the best of our knowledge, this is the first study in which two different markers to detect both perfusion and hypoxia have been used together in PET to assess cancer. Using the two radiotracers together was possible because of their relatively short half-life periods. By comparing the two scans for each patient in taking the ratio between ^{62}Cu-ATSM and ^{62}Cu-PTSM uptake rates to normalize ^{62}Cu-ATSM for ^{62}Cu-PTSM, we were able to obtain more information regarding hypoxic areas within the lesions than with the ^{62}Cu-ATSM scan alone. The ^{62}Cu-ATSM-to-^{62}Cu-PTSM ratio could possibly improve characterization of hypoxia, particularly in different areas of pulmonary lesions. New advances in MRI have produced dynamic contrast-enhanced MRI, which images tissue perfusion [16], as well as blood oxygen level–dependent MRI, which images changes in oxygenation [17]. Given the practical nature of PET in both cost and time efficiency when compared with MRI, we suggest that the ^{62}Cu-ATSM and ^{62}Cu-PTSM techniques provide a potentially clinically useful tool in imaging both tissue hypoxia and perfusion.

There was a steep learning curve during study implementation, which limited our ability to perform full analyses on all 10 patients who were originally enrolled. We realized during the study that a full analysis on hypoxia would necessitate sequences acquired over 20 minutes for each of the ^{62}Cu-ATSM and ^{62}Cu-PTSM PET scans. Because of claustrophobia and difficulty lying flat, one patient could not tolerate this extended duration of image acquisition for the full scans. These limitations restricted our analysis to only six patients.

Cytokine arrays were used to identify candidate protein targets in serum, with the aim of correlating serum markers with hypoxia or outcome. Several biomarkers showed large variability between patients, highlighting their potential for future studies, because ideal candidate biomarkers should show differences between populations to identify correlations with outcome [18]. Although our study was too small to draw conclusions about these biomarkers, a larger cohort may reveal trends correlating with hypoxia or survival. Moreover, evaluating additional markers, such as plasminogen activator inhibitor–1 and osteopontin, in conjunction with known survival signals such as VEGF may reveal a protein signature that identifies a relationship with hypoxia or clinical outcome [19].

There was interestingly a high degree of correlation between higher levels of tumor hypoxia, as evidenced by the ^{62}Cu-ATSM-to-^{62}Cu-PTSM ratios and lower EGF plasma levels. This finding suggests that more-hypoxic tumors may be less able to produce growth factor and, therefore, less able to signal by autocrine loops. The implication of lower EGF production, however, is still to be determined.

Furthermore, there were relatively higher plasma mean concentrations of VEGF and lower plasma mean concentrations of soluble FMS-like tyrosine kinase 1 to higher tumor hypoxia, as detected by ^{62}Cu-ATSM PET scans, although this correlation was unimpressive. VEGF

receptor–1 (also known as Flt-1) and VEGF receptor–2 (also known as KDR/Flk-1) have been found to be an essential regulatory system for angiogenesis; Flt-1 has been shown to have a negative regulatory function for angiogenesis, possibly because of its strong VEGF-trapping activity [20]. Our finding is supportive of the known inverse relationship between VEGF and Flt-1. Unexpectedly, the patient who had the most hypoxia on ^{62}Cu-ATSM scan had a sarcomatoid lung carcinoma and also had the lowest VEGF and soluble FMS-like tyrosine kinase 1 concentrations in our serum studies. This finding that high levels of tumor hypoxia were associated with low levels of VEGF and soluble FMS-like tyrosine kinase 1 is in contrast to previous studies in patients with non–small lung cancer that suggested that elevated serum VEGF levels are associated with higher levels of tumor hypoxia and portend poor prognosis [21]. Furthermore, because the overexpression of HIF-1 is known to increase VEGF levels, it is intriguing that we see the opposite trend with hypoxia detected by the ^{62}Cu-ATSM imaging technique. It is well established that hypoxia is a dynamic feature of the tumor microenvironment, which may contribute to this unexpected result [2]. Moreover, it is possible that the systemic concentrations of VEGF do not correlate with the concentration of VEGF seen in the tumor local environment.

Unlike the patient we reported with benign granuloma who had low ^{62}Cu-ATSM uptake [15], the patient with the nonmalignant inflammatory condition of pulmonary Langerhans cell histiocytosis also had tissue hypoxia on ^{62}Cu-ATSM and ^{62}Cu-PTSM scans. This tissue hypoxia was at a level similar to that shown by malignancies. Pulmonary Langerhans cell histiocytosis is an inflammatory condition in which histiocytes accumulate and produce local inflammation, resulting first in nodules and later organizing into fibrosis and cystic lesions [22]. In the earlier nodular phase, the cells at the center of the inflammation and granulomatous condition may be postulated to be more hypoxic, as seen on this series of scans.

With this experience of imaging tissue hypoxia and perfusion via ^{62}Cu-ATSM and ^{62}Cu-PTSM PET scans, we have shown the feasibility of obtaining both measurements of perfusion and tissue hypoxia in patients who have malignancies, as well as other hypoxic pathologic abnormalities, in a noninvasive manner. The ability to differentiate hypoxic tissue from normal tissue potentially may affect the predicting prognosis. Indeed, the importance of tumor hypoxia on prognosis has been shown by others on surgical pathology specimens, because hypoxia markers were associated with shorter survival [23]. Furthermore, this noninvasive imaging test for hypoxia could potentially become a surrogate for measuring tumor response to treatment and would pose a much lower risk but would provide similar valuable information that would otherwise necessitate biopsies in patients with pulmonary lesions. Finally, combining ^{62}Cu-ATSM and ^{62}Cu-PTSM scans and proteomics data may reveal a clinical signature related to hypoxia and clinical outcomes.

By understanding the distribution of tumor hypoxia in pulmonary lesions, we may find better predictors of recurrence and therapeutic targets in hypoxia pathways. This study highlights the need for further clinical trials of noninvasive testing to detect hypoxia in patients with lung cancer.

Acknowledgments

This work was supported in part by the National Cancer Institute (NCI) and Proportional Technologies (grant 5R44-CA110154-02) and the NCI (grant CA40355).

We thank Gregory Palmer and Jeffrey L. Lacy for their contributions.

References

1. Howlader, N.; Noone, AM.; Krapcho, M., et al. [Accessed December 10, 2012] National Cancer Institute. SEER cancer statistics review, 1975–2010. National Cancer Institute website. seer.cancer.gov/csr/1975_2010/
2. Bertout JA, Patel SA, Simon MC. The impact of O2 availability on human cancer. Nat Rev Cancer. 2008; 8:967–975. [PubMed: 18987634]
3. Dewhirst MW. Relationships between cycling hypoxia, HIF-1, angiogenesis and oxidative stress. Radiat Res. 2009; 172:653–665. [PubMed: 19929412]
4. Moon EJ, Brizel DM, Chi JT, Dewhirst MW. The potential role of intrinsic hypoxia markers as prognostic variables in cancer. Antioxid Redox Signal. 2007; 9:1237–1294. [PubMed: 17571959]
5. Kim SJ, Rabbani ZN, Vollmer RT, et al. Carbonic anhydrase IX in early-stage non-small cell lung cancer. Clin Cancer Res. 2004; 10:7925–7933. [PubMed: 15585626]
6. Lewis JS, Sharp TL, Laforest R, Fujibayashi Y, Welch MJ. Tumor uptake of copper-diacetyl-bis(N(4)-methylthiosemicarbazone): effect of changes in tissue oxygenation. J Nucl Med. 2001; 42:655–661. [PubMed: 11337556]
7. McCarthy DW, Bass LA, Cutler PD, et al. High purity production and potential applications of copper-60 and copper-61. Nucl Med Biol. 1999; 26:351–358. [PubMed: 10382836]
8. McCarthy DW, Shefer RE, Klinkowstein RE, et al. Efficient production of high specific activity ^{64}Cu using a biomedical cyclotron. Nucl Med Biol. 1997; 24:35–43. [PubMed: 9080473]
9. Green MA, Mathias CJ, Welch MJ, et al. Copper-62-labeled pyruvaldehyde bis(N4-methylthiosemicarbazonato)copper(II): synthesis and evaluation as a positron emission tomography tracer for cerebral and myocardial perfusion. J Nucl Med. 1990; 31:1989–1996. [PubMed: 2266398]
10. Anderson CJ, Connett JM, Schwarz SW, et al. Copper-64-labeled antibodies for PET imaging. J Nucl Med. 1992; 33:1685–1691. [PubMed: 1517844]
11. Xiao Z, Donnelly PS, Zimmermann M, Wedd AG. Transfer of copper between bis(thiosemicarbazone) ligands and intracellular copper-binding proteins: insights into mechanisms of copper uptake and hypoxia selectivity. Inorg Chem. 2008; 47:4338–4347. [PubMed: 18412332]
12. Takahashi N, Fujibayashi Y, Yonekura Y, et al. Evaluation of ^{62}Cu labeled diacetyl-bis(N4-methylthiosemicarbazone) as a hypoxic tissue tracer in patients with lung cancer. Ann Nucl Med. 2000; 14:323–328. [PubMed: 11108159]
13. Dehdashti F, Grigsby PW, Lewis JS, Laforest R, Siegel BA, Welch MJ. Assessing tumor hypoxia in cervical cancer by PET with ^{60}Cu-labeled diacetyl-bis(N4-methylthiosemicarbazone). J Nucl Med. 2008; 49:201–205. [PubMed: 18199612]
14. Dehdashti F, Mintun MA, Lewis JS, et al. In vivo assessment of tumor hypoxia in lung cancer with ^{60}Cu-ATSM. Eur J Nucl Med Mol Imaging. 2003; 30:844–850. [PubMed: 12692685]
15. Wong TZ, Lacy JL, Petry NA, et al. PET of hypoxia and perfusion with ^{62}Cu-ATSM and ^{62}Cu-PTSM using a ^{62}Zn/^{62}Cu generator. AJR. 2008; 190:427–432. [PubMed: 18212229]
16. Zhao B, Schwartz LH, Larson SM. Imaging surrogates of tumor response to therapy: anatomic and functional biomarkers. J Nucl Med. 2009; 50:239–249. [PubMed: 19164218]
17. Zhao D, Jiang L, Hahn EW, Mason RP. Comparison of ^{1}H blood oxygen level-dependent (BOLD) and ^{19}F MRI to investigate tumor oxygenation. Magn Reson Med. 2009; 62:357–364. [PubMed: 19526495]
18. Lee JW, Figeys D, Vasilescu J. Biomarker assay translation from discovery to clinical studies in cancer drug development: quantification of emerging protein biomarkers. Adv Cancer Res. 2007; 96:269–298. [PubMed: 17161683]

19. Goudar RK, Vlahovic G. Hypoxia, angiogenesis, and lung cancer. Curr Oncol Rep. 2008; 10:277–282. [PubMed: 18778551]

20. Hiratsuka S, Maru Y, Okada A, et al. Involvement of Flt-1 tyrosine kinase (vascular endothelial growth factor receptor-1) in pathological angiogenesis. Cancer Res. 2001; 61:1207–1213. [PubMed: 11221852]

21. Bremnes RM, Camps C, Sirera R. Angiogenesis in non-small cell lung cancer: the prognostic impact of neoangiogenesis and the cytokines VEGF and bFGF in tumours and blood. Lung Cancer. 2006; 51:143–158. [PubMed: 16360975]

22. Allen TC. Pulmonary Langerhans cell histiocytosis and other pulmonary histiocytic diseases: a review. Arch Pathol Lab Med. 2008; 132:1171–1181. [PubMed: 18605769]

23. Kim SJ, Rabbani ZN, Dewhirst MW, et al. Expression of HIF-1alpha, CA IX, VEGF, and MMP-9 in surgically resected non-small cell lung cancer. Lung Cancer. 2005; 49:325–335. [PubMed: 15935515]

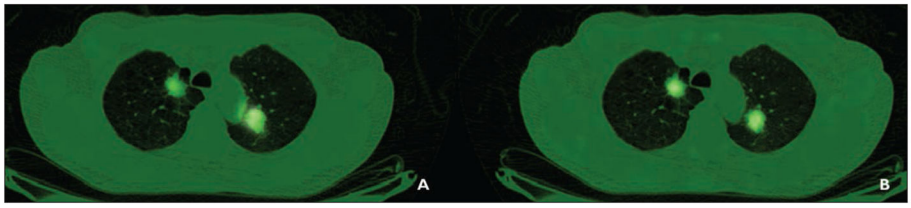

Fig. 1.

64-year-old man with adenocarcinoma (patient 3).

A and **B,** Representative copper-pyruvaldehyde-bis(N4-methylthiosemicarbazone) (**A**) and copper-diacetyl-bis(N4-methylthiosemicarbazone) (**B**) images of bilateral lung nodules are shown.

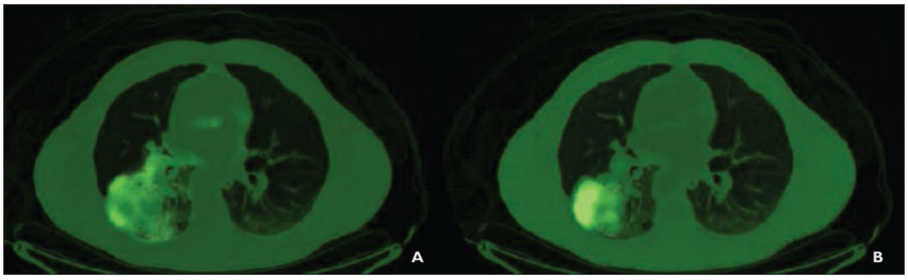

Fig. 2.

63-year-old man with sarcomatoid carcinoma of lung (patient 5).

A and **B,** Copper-pyruvaldehyde-bis(N4-methylthiosemicarbazone) (**A**) and copper-diacetyl-bis(N4-methylthiosemicarbazone) (**B**) images of right lower lobe mass are shown.

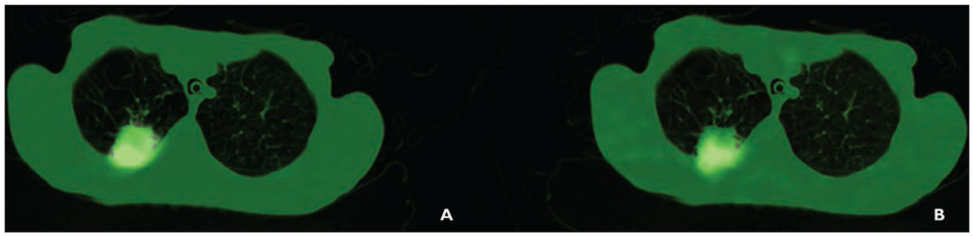

Fig. 3.

54-year-old woman with adenocarcinoma (patient 6).

A and **B,** Images of right middle lobe lesion using copper-pyruvaldehyde-bis(N4-methylthiosemicarbazone) (**A**) and copper-diacetyl-bis(N4-methylthiosemicarbazone) (**B**) are shown.

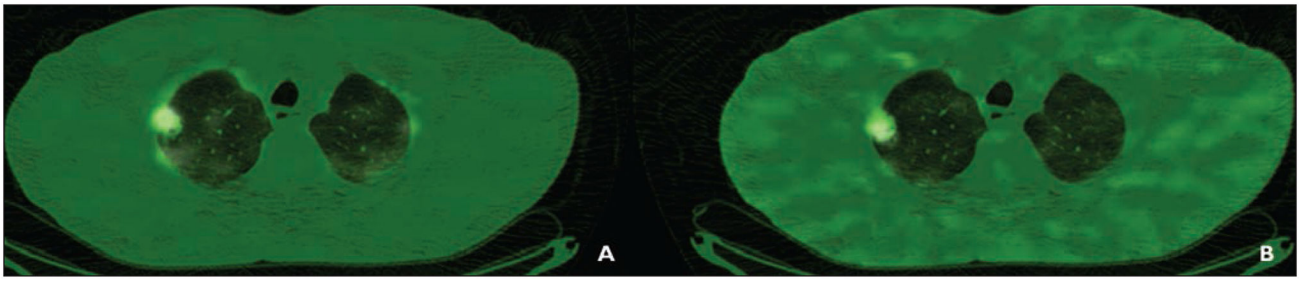

Fig. 4.

53-year-old man with pulmonary Langerhans cell histiocytosis (patient 8).

A and **B,** Representative images of copper-pyruvaldehyde-bis(N4-methylthiosemicarbazone) (**A**) and copper-diacetyl-bis(N4-methylthiosemicarbazone) (**B**) are shown.

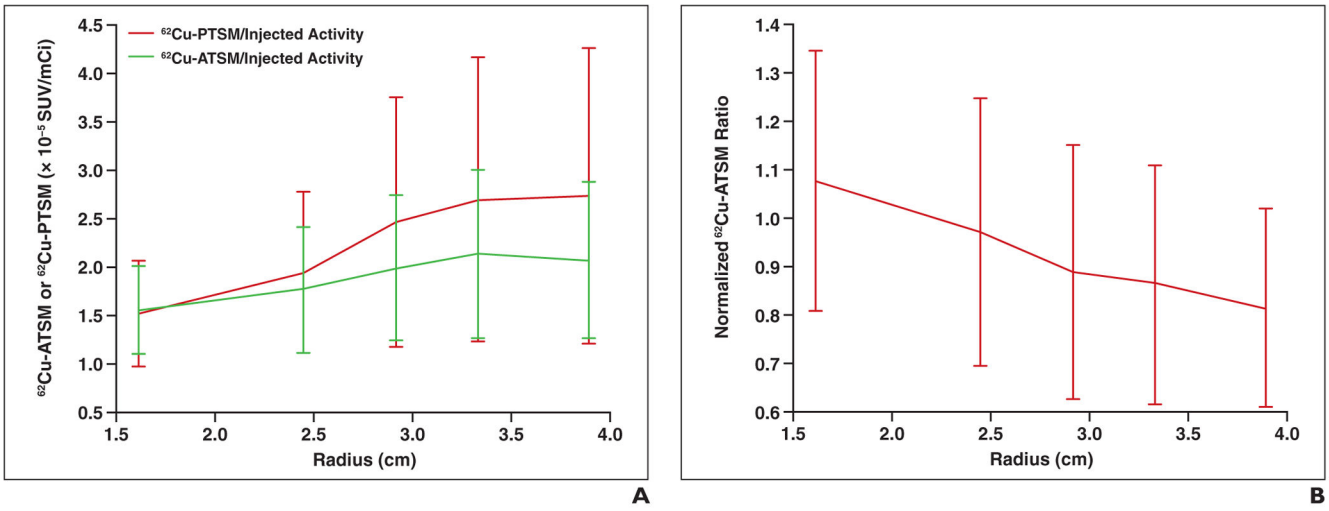

Fig. 5.

63-year-old man (patient 5).

A, Graph shows copper-diacetyl-bis(N4-methylthiosemicarbazone) (^{62}Cu-ATSM) and copper-pyruvaldehyde-bis(N4-methylthiosemicarbazone) (^{62}Cu-PTSM) as function of distance from center of tumor. SUV = standardized uptake value.

B, Graph shows normalized ^{62}Cu-ATSM-to-^{62}Cu-PTSM ratio as function of distance from center of tumor.

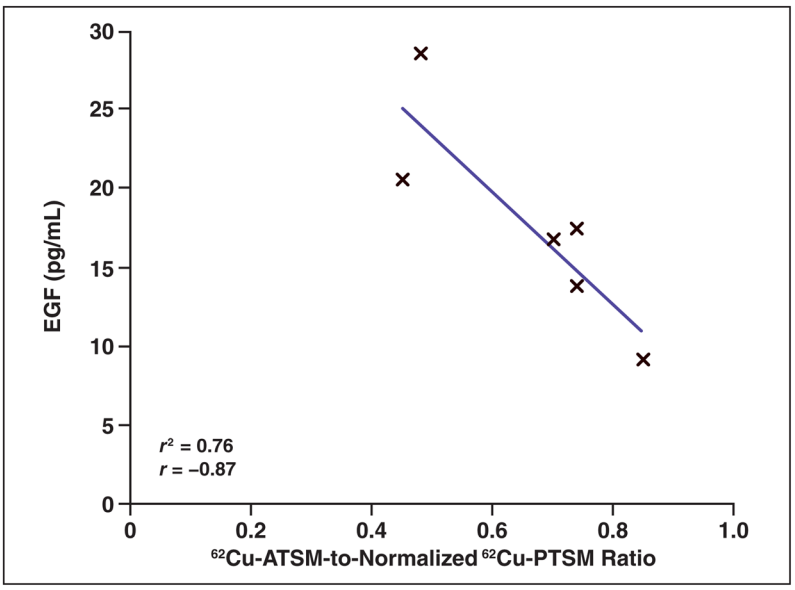

Fig. 6.

Epidermal growth factor (EGF) had highest correlation with tumor hypoxia. As tumor hypoxia increases as measured by ratio of copper- diacetyl-bis(N4-methylthiosemicarbazone) (^{62}Cu-ATSM) to copper-pyruvaldehyde-bis(N4-methylthiosemicarbazone) (^{62}Cu-PTSM), plasma mean concentration of EGF decreases.

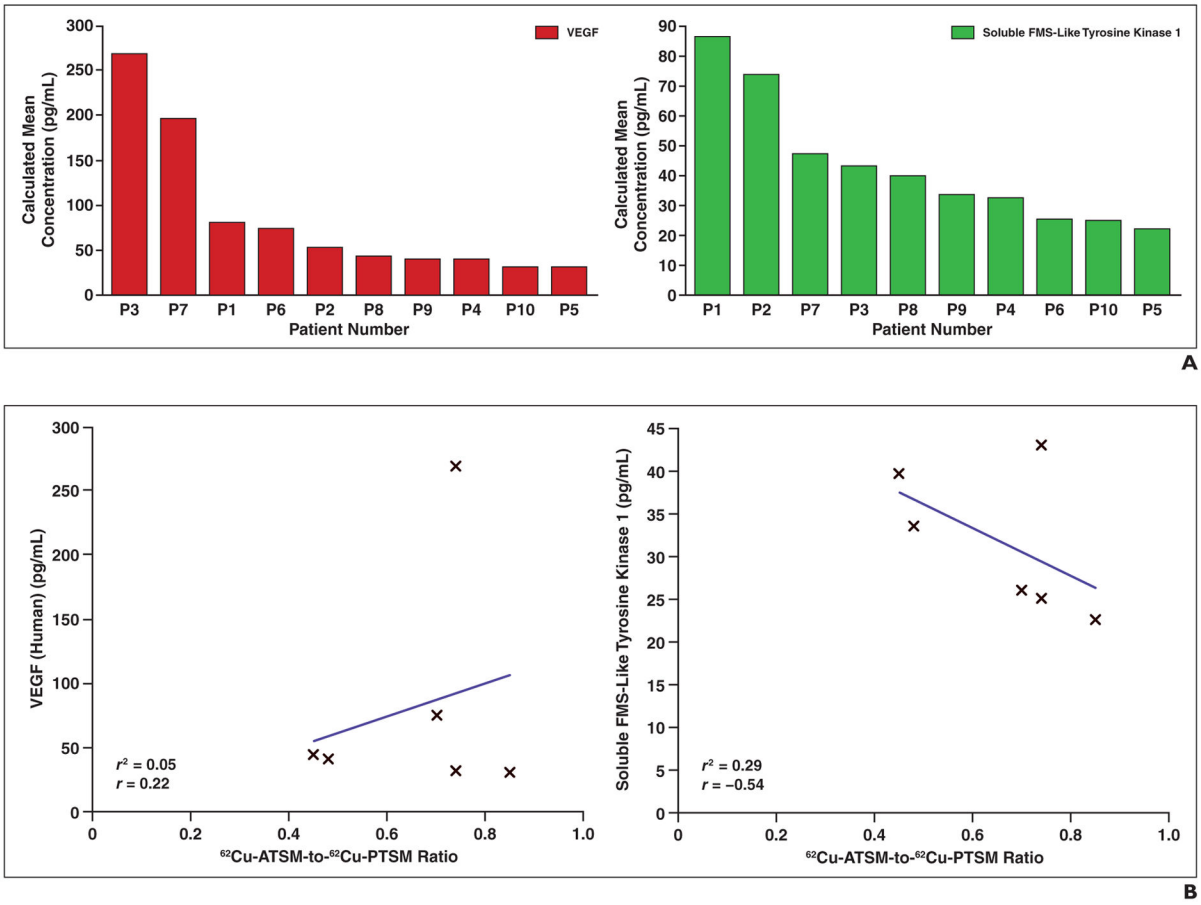

Fig. 7.

Vascular endothelial growth factor (VEGF) and soluble FMS-like tyrosine kinase 1 plasma concentrations.

A, Waterfall plots of VEGF (*left*) and soluble FMS-like tyrosine kinase 1 (*right*) plasma calculated mean concentrations reveal large range of values in patient population.

B, Higher plasma mean concentrations of VEGF (*left*) and lower mean plasma concentrations of soluble FMS-like tyrosine–1 (*right*) correlate with higher tumor hypoxia as detected by copper-diacetyl-bis(N4-methylthiosemicarbazone) (^{62}Cu-ATSM) and copper-pyruvaldehyde-bis(N4-methylthiosemicarbazone) (^{62}Cu-PTSM) PET scans.

TABLE 1

Patient Demographics With Surgical Pathologic Diagnosis, Tumor Staging, and Survival Data

Characteristic	Patient 1	Patient 2	Patient 3	Patient 4	Patient 5	Patient 6	Patient 7	Patient 8	Patient 9	Patient 10
Sex	Female	Male	Male	Male	Male	Female	Male	Male	Male	Male
Age (y)	71	59	64	60	63	54	70	53	66	72
Weight (kg)	70.5	65.5	67	91.4	74.5	36.9	70.7	65.1	100.6	96
Height (cm)	Unknown	175	176	181	176	152	178	163	177	171
Body mass index (kg/m^2)		21.4	21.6	27.9	24.1	16.0	22.3	24.5	32.1	32.8
Pathologic diagnosis	Adenocarcinoma	Granuloma	Adenocarcinoma	Head and neck squamous cell carcinoma	Sarcomatoid carcinoma of lung	Adenocarcinoma	Adenocarcinoma	Pulmonary Langerhans cell histiocytosis	Adenocarcinoma	Adenocarcinoma
Stage			IV	IV	III	III	IV	Unstaged	II	I
Survival (mo)			14	5	5	4	15	> 24	> 24	> 24

TABLE 2

Tumor Standardized Uptake Values (SUVs) for ^{18}F-FDG, Copper-Diacetyl-Bis(N4-Methylthiosemicarbazone) (^{62}Cu-ATSM), and Copper-Pyruvaldehyde-Bis(N4-Methylthiosemicarbazone) (^{62}Cu-PTSM)

Characteristic	Patient 1[a]	Patient 2 [a]	Patient 3	Patient 4 [a]	Patient 5	Patient 6	Patient 7[b]	Patient 8	Patient 9	Patient 10
Tumor location, size			LUL, 7.11 cm^3; RUL, 3.81 cm^3		RLL, 206.8 cm^3	RUL, 5.44 cm^3		RUL, 0.36 cm^3	RUL, 17.71 cm^3	RUL, 2.91 cm^3
FDG										
Maximum SUV	10.5	8.4	LUL, 12.1; RUL, 17.6	15.0	NA[c]	7.1	10.1	5.5	9.1	LUL, 17.0; RUL, 16.6
Dose (mCi) [MBq]	10.4 [384.8]	10.0 [370.0]	12.3 [455.1]	16.3 [603.1]	14.2 [525.4]	10.0 [370.0]	13.1 [484.7]	11.4 [421.8]	13.5 [499.5]	
Time between FDG PET and ^{62}Cu-PET studies	> 30 d	27 d	1 h	5 h	11 d	1 h	2 h	1 h	1 h	1 h
^{62}Cu-PTSM										
Dose (mCi) [MBq]	3.76 [139.12]	8.9 [329.3]	8.18 [302.66]	9.75 [360.75]	13.9 [514.3]	5.07 [187.59]	14.29 [528.73]	12.76 [472.12]	16.34 [604.58]	16.01 [592.37]
SUV for tumor	3.63	1.73	16.1	7.5	15.9	15.9	27.1	22.4	61.1	27.8
^{62}Cu-ATSM										
Dose (mCi) [MBq]	6.87 [254.19]	8.3 [307.1]	7.55 [279.35]	9.1 [336.7]	14.75 [545.75]	14.54 [537.98]	NA	13.86 [512.82]	14.46 [535.02]	13.62 [503.94]
SUV for tumor	2.71	1.00	9.8	5.1	13.2	36.6	NA	17.2	37.3	16

Note—LUL3= left upper lobe, NA3= not applicable, RLL3= right lower lobe, RUL3= right upper lobe.

[a] Patients whose imaging scans were not complete enough to calculate ^{62}Cu-ATSM and ^{62}Cu-PTSM differences.

[b] Patient did not complete ^{62}Cu-ATSM imaging.

[c] Patient whose PET scan was performed before initial medical evaluation at our hospital, and SUV was not reported.

TABLE 3

Characteristics of Six Patients Who Completed Copper-Diacetyl-Bis(N4-Methylthiosemicarbazone) (^{62}Cu-ATSM) and Copper-Pyruvaldehyde-Bis(N4-Methylthiosemicarbazone) (^{62}Cu-PTSM) Imaging

Patient	^{62}Cu-ATSM-to-^{62}Cu-PTSM Ratio[a]	Pathologic Diagnosis	Stage	Survival (mo)
3	0.77, left lower lobe; 0.71, right upper lobe	Adenocarcinoma	IV	14
5	0.85	Sarcomatoid carcinoma	III	5
6	0.70	Adenocarcinoma	III	4
8	0.45	Pulmonary Langerhans cell histiocytosis	Unstaged	> 24
9	0.48	Adenocarcinoma	II	> 24
10	0.74	Adenocarcinoma	I	> 24

[a]This ratio was taken as the sum of all the ^{62}Cu-ATSM-to-^{62}Cu-PTSM ratios for all voxels divided by the number of voxels, as described in the Subjects and Methods section.